A Power Balanced Dual-Wavelength Nd:$GdVO_4$ Laser With 0.6 THz Frequency Separation

Yuting Zhang, Miao Hu, Mengmeng Xu, Hengfeng Yan, Chong Liu, Long Chen, Haozhen Li, Meihua Bi, and Xuefang Zhou

***Abstract*—A power balanced dual-wavelength laser (DWL) based on the Nd:$GdVO_4$ crystal is presented. The orthogonally polarized gain spectral evolution of the Nd:$GdVO_4$ crystal versus the temperature is studied, and the power balancing conditions of the DWLs are theoretically analyzed firstly. In the experiments, by using two output couplers and a temperature controller, the power balanced Nd:$GdVO_4$ DWL signals at 1063 nm (π) and 1065 nm (σ) are obtained with the crystal heat sink temperature (T_c) from 20 °C to 40 °C. The experimental results show, with the pump power at 9.3 W and T_c at 25 °C, the DWL signal of the balanced power at 0.78 W for each wavelength and the frequency separation at 0.62 THz is realized. The beam quality M^2 of the π- and σ-polarized DWL signals are measured between 2.1 to 2.4.**

***Index Terms*—Terahertz wave, dual-wavelength laser, power balanced.**

I. Introduction

OVER the past decades, simultaneous dual-wavelength lasers (DWLs) exhibit a variety of applications, such as optical radio frequency waves generation [1]–[3], medical diagnosis [4]–[6], holographic interferometry [7], [8], lidar [9]–[11] and so on. In particular, the DWLs with the frequency separations between 0.1 and 10 THz, generate terahertz waves by utilizing photo-conductive switches or nonlinear crystals [12]–[15], and therefore become the promising optical sources in terahertz communications, spectroscopy, imaging systems and so on [16]. The Nd-doped vanadate crystals, which are characterized with high absorption cross sections, large stimulated emission cross sections (ECS) and natural birefringences, are favorable for the DWLs with THz frequency separations. For instance, based on the etalon effect, A Mckay obtained a 20 mW DWL signal with frequency separation at 0.15 THz by using a monolithic microchip Nd:YAG crystal [17]. Y. P. Huang designed a Nd:$LuVO_4$ DWL with wavelengths at 1086 and 1089 nm by inserting an etalon with free spectral range (FSR) at 0.71 THz [18]. Also, by employing the dual-gain spectral peaks of the Nd-doped vanadate crystals, Pu Zhao achieved a Nd:YLF DWL with the output power of 1.196 W at 1047 nm and 0.608 W at 1053 nm, the frequency separation was 1.64 THz [13]. Wu Bo obtained a Nd:$GdVO_4$ DWL with output power of 4.0 W at 1065.5 nm and 1.0 W at 1063.1 nm, the frequency separation was 0.63 THz [19].

By employing the DWL signal for heterodyne frequency beating, since the DWL power balance degree is an important factor for the beat-noting efficiency, many researches on the power balanced DWL have been carried out. Florent Pallas achieved the dual-wavelength emission with balanced output power of 200 mW by tilting the output coupler in a c-cut Nd:$GdVO_4$ laser [20]. However, due to the tilting angle limitation, the power balance degree of the DWL was technically not adjustable. H. C. Liang adjusted the output power balance degree of the DWL by varying the radius of curvature of the input coupler in a Nd:YLF laser [21]. The large radius curvature of the input coupler easily led the DWL cavity to be unstable and the power balance degree was only roughly adjusted yet.

Since the output powers of the two wavelength components in the DWL primarily due to the wavelength dependent ECS values of the gain medium, the output power balance degree of the DWL is adjusted by the tuning the ECS spectra. Also, by considering the natural thermal characteristics of the Nd-doped vanadate crystals, the ECS spectra of the laser gain medium can be tuned by the temperature variation of the gain medium [22].

In this work, the Nd:$GdVO_4$ DWL with 0.6 THz frequency separation is demonstrated. The temperature dependent ECS spectra of the Nd:$GdVO_4$ crystal are analyzed in Section II. The power balanced conditions are theoretically analyzed, and the experiment setup is shown in Section III. The experimental results are disscussed in Section IV. The conclusions are given in Section V.

II. The Nd:$GdVO_4$ Emission Cross Section Spectra From 20 °C to 60 °C

To obtain the temperature dependent ECS spectra of the Nd:$GdVO_4$ crystal, the crystal is placed in a copper heat sink and the orthogonally polarized fluorescence spectra are recorded

Manuscript received 10 May 2022; revised 22 June 2022; accepted 10 July 2022. Date of publication 14 July 2022; date of current version 24 August 2022. This work was supported in part by the Primary Research and Development Plan of Zhejiang Province under Grant 2020C01106, in part by the National Natural Science Foundation of China under Grant 61705055, and in part by the Fundamental Research Funds for the Provincial Universities of Zhejiang under Grant GK209907299001-018. *(Corresponding author: Miao Hu.)*

Yuting Zhang, Miao Hu, Mengmeng Xu, Haozhen Li, Meihua Bi, and Xuefang Zhou are with the College of Communication Engineering, Hangzhou Dianzi University, Hangzhou 310018, China (e-mail: YutingZhang@163.com; miao_hu@foxmail.com; xumengmeng@hdu.edu.cn; haozhenli@hdu.edu.cn; bmhua@hdu.edu.cn; zhouxf@hdu.edu.cn).

Hengfeng Yan is with the Changzhou Inno Laser Technology Corporation Limited, Changzhou 213164, China (e-mail: yanhengfeng@inno-laser.com).

Chong Liu is with the College of Optical Science and Engineering, Zhejiang University, Hangzhou 310027, China (e-mail: chongliu@zju.edu.cn).

Long Chen is with the Zhejiang Dongtong Optical Network and IOT Technology Company, Ltd., Huzhou 313009, China (e-mail: chenlongts@htgd.com.cn).

Digital Object Identifier 10.1109/JPHOT.2022.3190610

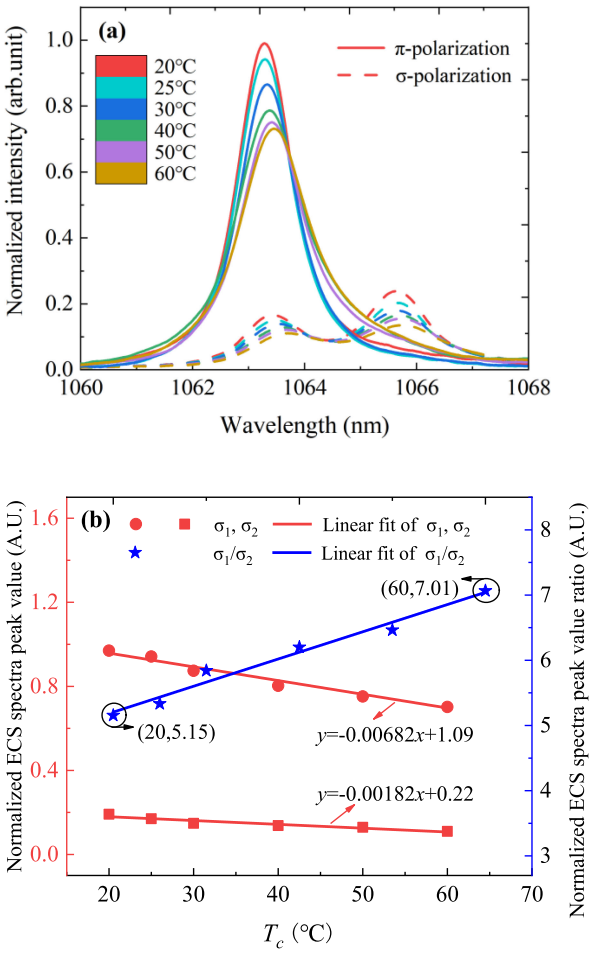

Fig. 1. (a) The normalized temperature dependent fluorescence spectra of the Nd:$GdVO_4$ crystal with T_c from 20 to 60 °C. (b) The normalized ECS spectral peak value ratio versus T_c.

by an optical spectrum analyzer. Fig. 1(a) shows the normalized temperature dependent fluorescence spectra in π- and σ-polarizations of the Nd:$GdVO_4$ crystal. The solid and dash curves represent the π- and σ-polarizations, the different colors represent the different heat sink temperature T_c, respectively. The fluorescence spectra with T_c from 20 °C to 60 °C are shown in Fig. 1(a) over the spectral range from 1060 nm to 1068 nm. For each T_c, the fluorescence spectra have three peaks, the peak wavelengths locate at 1063 nm in π- and σ-polarizations, at 1065 nm in σ-polarization. By employing the Fuchtbauer-Ladenburg equations [23], the expression of the temperature dependent ECS spectrum is expressed as:

$$\sigma_i(\lambda,\ T_c) = \frac{(\overline{\lambda_i})^4}{8\pi c n_i^2 \tau_i} \frac{I_i(\lambda,\ T_c)}{\int I_i(\lambda,\ T_c) d\lambda}, i = 1, 2, \qquad (1)$$

where $\sigma_i(\lambda,T_c)$ is the temperature dependent ECS spectrum, $I_i(\lambda,T_c)$ is the temperature dependent fluorescence spectrum, τ_i is the fluorescence lifetime, n_i is the optical index, $\bar{\lambda}_i$ is the average emission wavelength. Here, $i = 1,2$ represent the wavelengths of 1063 nm (π) and 1065 nm (σ). Since the refractive index and the fluorescence lifetime of the Nd:$GdVO_4$ crystal stay constant over the range of the temperature [24], by (1), the $\sigma_i(\lambda,T_c)$ evolution only depends on the $I_i(\lambda,T_c)$.

The relationship between the ECS of 1063 nm in π-polarization and 1065 nm in σ-polarization are analyzed in depth. Within T_c increasing from 20 °C to 60 °C, the π-polarized ECS spectral peak wavelength shifts from 1063.28 nm to 1063.44 nm and the σ-polarized ECS spectral peak wavelength shifts from 1065.64 nm to 1065.77 nm, the wavelength separation between the two peaks is about 2.3 nm. The relationship between the normalized ECS spectral π peak to σ peak value ratio versus T_c is shown in Fig. 1(b). σ_1 and σ_2 represent the normalized ECS spectral peak values of the π- and σ-polarizations. σ_1/σ_2 is the peak value ratio. Within T_c from 20 °C to 60 °C, σ_1 and σ_2 linearly decrease with the slope of 0.682%/ °C and 0.182%/ °C, σ_1/σ_2 increases linearly from 5.15 to 7.01.

III. Theoretical Analysis and Experimental Setup

A. Theoretical Analysis for the Balanced Power DWL Operation in Different T_c

Based on the space-dependent rate equation [25], the pump threshold ratio between the two wavelengths is expressed as:

$$\frac{P_{th,2}}{P_{th,1}} = \frac{\ln\left(\frac{1}{R_{oc,2}}\right) + \delta_2}{\ln\left(\frac{1}{R_{oc,1}}\right) + \delta_1} \frac{\sigma_1(T_c)}{\sigma_2(T_c)}, \qquad (2)$$

where $P_{th,}$ R_{oc} and δ are parameters of the pump threshold, the output coupler reflectivity and the geometric deflection loss of the laser cavity, respectively. With the similar cavities, the geometric deflection losses of δ_1 and δ_2 are reasonably considered to be equal as the same loss δ. Therefore, the pump threshold ratio $P_{th,2}$ /$P_{th,1}$ depends on the output coupler reflectivity R_{oc} and the temperature dependent ECS spectral peak value $\sigma(T_c)$.

Further, according to the diode-end-pumped laser equation [26], the slope efficiency S_e and the output power P_{out} for the specific emission line of the DWL are expressed as:

$$S_{e,i} = \frac{\ln\left(\frac{1}{R_{oc,i}}\right)}{\ln\left(\frac{1}{R_{oc,i}}\right) + \delta_i} \eta_{q,i} \frac{\lambda_p}{\lambda_i} \frac{[\int\int\int s_i(r,z) r_p(r,z) dv]^2}{\int\int\int s_i^2(r,z) r_p(r,z) dv}, \qquad (3)$$

$$P_{out,i} = s_{e,i}(P_{in} - P_{th,i}), \qquad (4)$$

where the parameters $\eta_{q,i}$, $h\nu_p$, s_i(r,z) and r_p(r,z) are the quantum efficiency, the pump photon energy, the normalized cavity mode intensity distribution and the normalized pump intensity distribution. The subscript i represents the corresponding laser wavelength of the DWL, the parameters λ_p and P_{in} are the pump wavelength and the incident pump power. Since the two close wavelength lasers are pumped by the same pump source and transmit between the same upper and lower level, with the similar laser cavities, the parameters $\eta_{q,i}$, λ_p, s_i(r,z) and r_p(r,z) of the two wavelengths are reasonably considered to be equal. Therefore, the difference of the slope efficiency $S_{e,i}$ of the two wavelengths only depends on the parameter of $R_{oc,i}$.

Assumption 1 is that the output coupler reflectivity R_{oc} at 1063 and 1065 nm are the same, i.e., $R_{oc,1} = R_{oc,2}$. Since the ECS

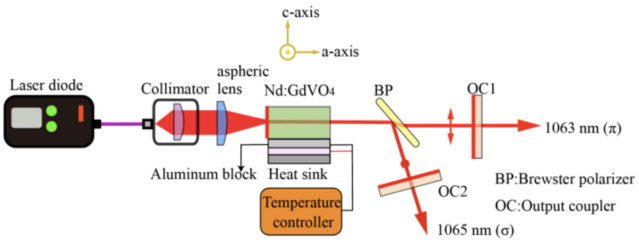

Fig. 2. The experimental setup of the Nd:GdVO$_4$ DWL.

value $\sigma_1(T_c)>\sigma_2(T_c)$, according to (2), it is easily deduced that $P_{th,2}>P_{th,1}$. The result of $P_{th,2}>P_{th,1}$ indicates the DWL first emits at 1063 nm. Also, since the output coupler reflectivity $R_{oc,1} = R_{oc,2}$, as P_{in} increases the output power $P_{out,1}$ and $P_{out,2}$ increase at the same slope efficiency S_e, which means $S_{e,1} = S_{e,2}$. Therefore, if the pump threshold $P_{th,2}$ is higher than $P_{th,1}$, under the premise of the same slope efficiency $S_{e,1} = S_{e,2}$, the power balancing is impossibly realized at any pump power.

Assumption 2 is that the output coupler reflectivity $R_{oc,1}\neq R_{oc,2}$, considering the ECS value $\sigma_1(T_c)>\sigma_2(T_c)$, it is consequently necessary to choose the output coupler with high reflectivity at 1065 nm and low reflectivity at 1063 nm. By using the appropriate output coupler reflectivities $R_{oc,2}$ and $R_{oc,1}$, the conditions of $R_{oc,2}>R_{oc,1}$ and $P_{th,2}<P_{th,1}$ are satisfied. With P_{in} increases, the laser first emits at 1065 nm then simultaneously emits at 1063 nm. Since the output coupler reflectivity $R_{oc,2}>R_{oc,1}$, according to (3), it is deduced that the slope efficiencies $S_{e,2}<S_{e,1}$. Hence, as P_{in} increases, it is always achieved a balanced power DWL operation above the threshold. In addition, under the condition of assumption 2, by slight adjusting the cavity lengths, the geometric deflection losses of δ_1 and δ_2 change accordingly, thereby the pump threshold ratio $P_{th,2}/P_{th,1}$ can be finely adjusted.

B. Experimental Setup

The experimental setup is shown in Fig. 2. A 400 μm multimode fiber-coupled laser diode with a wavelength of 808 nm is collimated and focused into the Nd:GdVO$_4$ crystal by a pair of aspheric lens. The focal length ratio between the collimating and focusing aspheric lens is 2:1. The gain medium is an a-cut, 1.0 at. % Nd:GdVO$_4$ crystal with the dimension of 3 × 3 × 3 mm^3. The front surface of the Nd:GdVO$_4$ crystal is coated high reflectively (HR) at 1064 nm and anti-reflectively (AR) at 808 nm. The rear surface of the crystal is coated HR at 808 nm and AR at 1064 nm. An intracavity Brewster polarizer (BP) separates the two orthogonally polarized laser beams to the respective output couplers. The 1063 nm laser beam of the DWL is π-polarization, and the 1065 nm laser beam is σ-polarization. The front surface of the BP is coated AR at 1064 nm. The end surface of the BP has a coating in such a way that when being placed at a Brewster angle (55.4 °) relative to the input beam, the π-polarized beam has a high transmittance of $T_p = 98\%$ at 1064 nm, whereas the σ-polarized beam has the high reflectivity of $R_s > 99.9\%$ at 1064 nm. The dimension of the BP is 25.4 × 25.4 × 3 mm^3. The material of the BP is Corning 7980 with the optical index of 1.45. The reflectivity of the two output couplers at 1063 nm (OC1) and 1065 nm (OC2) are R = 60% and R = 95% at 1064 nm, according to the theoretical analysis in Section III. The cavity lengths are designed to 45 mm at 1063 nm and 1065 nm. In the experiment, the actually used cavity lengths can be appropriately shortened or lengthened to decrease or increase the laser threshold.

To get better thermal contact and proper temperature control of the Nd:GdVO$_4$ crystal. A thermoelectric cooler (TEC) precisely controls the temperature (T_c) of the crystal heat sink. Meanwhile, the heating surface of the TEC is placed close to a water-cooled aluminum base for heat dissipation. Owing to the combination of the temperature controlling system, the T_c change range varies from 0 °C to 100 °C, and the controlling accuracy is ±0.1 °C. The output DWL signal separately feeds into a power meter (PM100A, THORLABS.) and a high-resolution (0.01 nm) optical spectrum analyzer (OSA, Q8384, Advantest.) for powers and optical spectra measurements.

IV. Experimental Results and Discussion

The DWL output powers versus the pump power with T_c in the range of 20 °C to 40 °C are presented. The output powers of π- and σ-polarized laser signals and the total output power versus the pump powers under different T_c are shown in Fig. 3. In all T_c, the σ-polarized 1065 nm light lases prior to the π-polarized 1063 nm light, and the balanced DWL signals are always achieved with the pump power increasing. As T_c increases from 20 °C to 40 °C, the maximum balanced output power is 0.78 W × 2 with the pump power of 9.3 W and T_c of 25 °C. The maximum total output power is 1.75 W with the pump power of 11.1 W and T_c of 25 °C, the total output power optical-to-optical slope efficiency is up to 15.2%.

Since the Nd:GdVO$_4$ crystal ECS spectral peaks linearly decrease as T_c increases, the threshold pump powers $P_{th,1}$ and $P_{th,2}$ increase as T_c increases. However, Fig. 3(e) shows the $P_{th,2}$ increasing and the $P_{th,1}$ decreasing as T_c increases. A good explanation is modes competition between the two wavelength components. Further, as shown in Fig. 3(b), for $T_c = 25$ °C, the output power of the σ-polarized 1065 nm light initially increases linearly as the pump power increases from 2.3 W ($P_{th,2}$), and reach its maximum power of 0.88 W with the pump power of 7.9 W. When the pump power continues to increase to 6.2 W ($P_{th,1}$), the π-polarized 1063 nm light starts to increase as the pump power increases. The gain competition between the π- and σ-polarized laser leads to the output power of the 1065 nm light decreases when the pump power exceeds 7.9 W, and the output power of the 1063 nm light rises with higher slope efficiency. The balanced output power of 0.78 W × 2 is obtained with the pump power of 9.3 W. Similar laser performances are observed for other T_c, as shown in Fig. 3(a), (c) and (d). The relationship between the threshold pump powers P_{th} and the pump powers at the power balanced points $P_{in,\,bal}$ versus T_c are shown in the Fig. 3(e). As T_c increases from 20 °C to 40 °C, the $P_{in,\,bal}$ linearly decreases from 9.5 W to 7.1 W with a slope of −0.13 W/ °C. The $P_{th,1}$ linearly decreases from 6.4 W to 5.8 W with

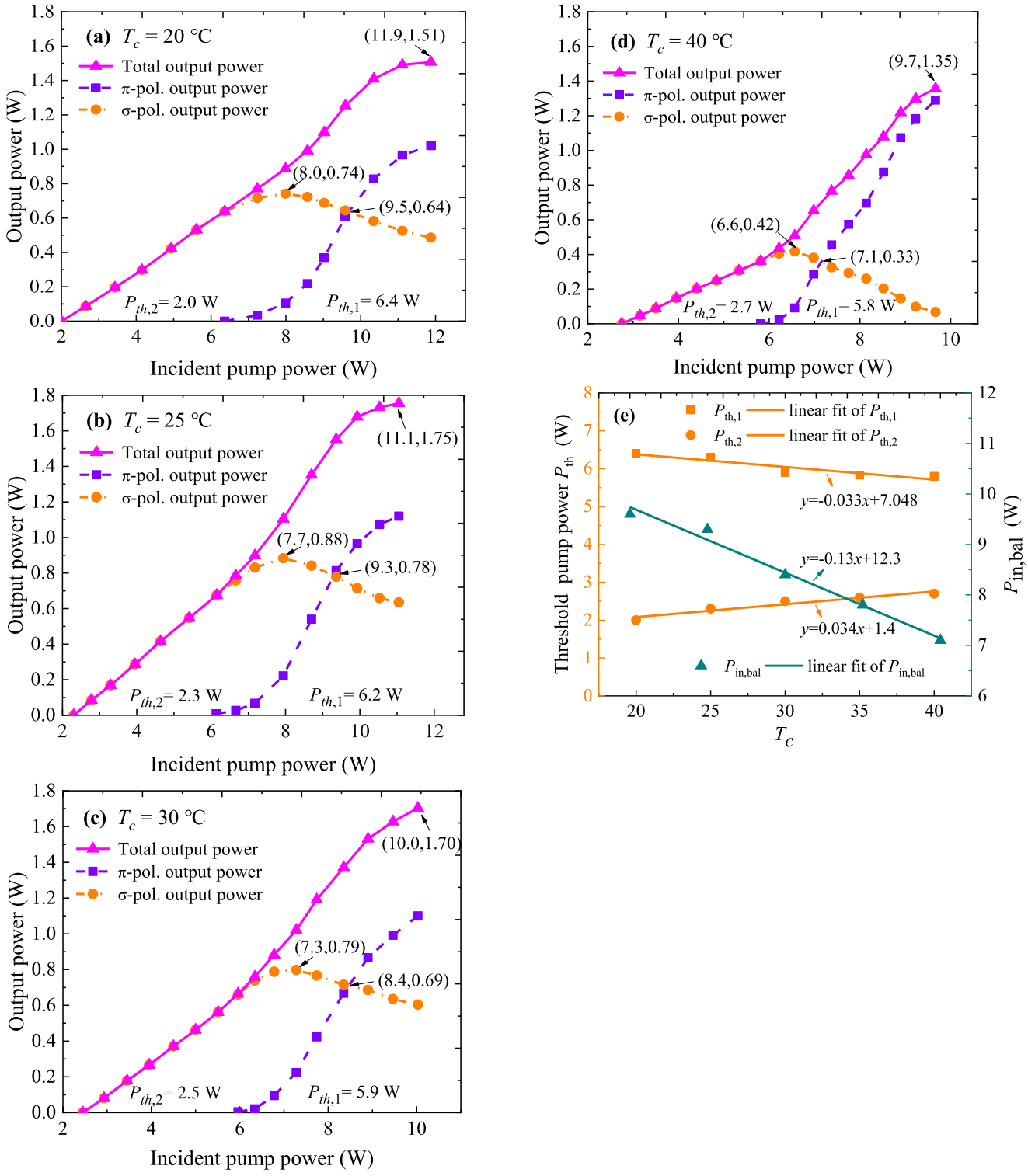

Fig. 3. The output power for π- and σ-polarized laser signals and the total output power versus the pump power under different T_c: (a) T_c = 20 °C. (b) T_c = 25 °C. (c) T_c = 30 °C. (d) T_c = 40 °C. (e) The P_{th} and the $P_{in,bal}$ of the DWL versus T_c.

a slope of -0.033 W/ °C and the $P_{th,2}$ linearly increases from 2.0 W to 2.7 W with a slope of 0.034 W/ °C. The experimental results agree with the theoretical analysis well.

The output beam qualities of the two orthogonally polarized outputs with the pump power of 9.3 W and T_c of 25 °C are experimentally observed, as shown in Fig. 4. The output beam distributions were measured by the camera beam profiler (BC106N-VIS/M, THORLABS.). By fitting the standard Gaussian beam propagation expression to the measured data, the M^2 factor values in x and y directions are calculated to be 2.26 and 2.12 for the π-polarized light, 2.42 and 2.21 for the σ-polarized light. The different M^2 values in the x and y directions of the

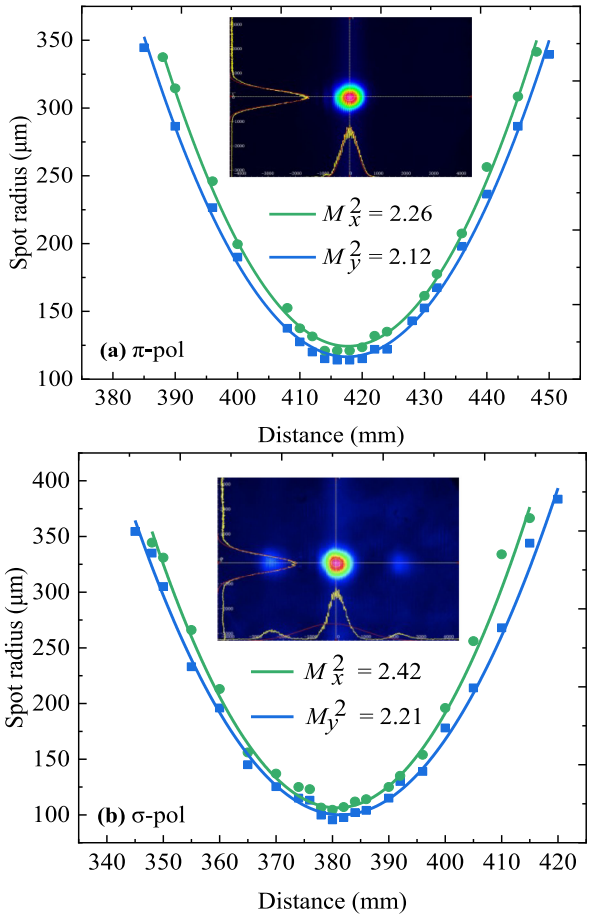

Fig. 4. The laser beam qualities of the π-polarized (a) and σ-polarized (b) laser with the pump power of 9.3 W and T_c of 25 °C. The insets show the output beam transverse intensity profiles.

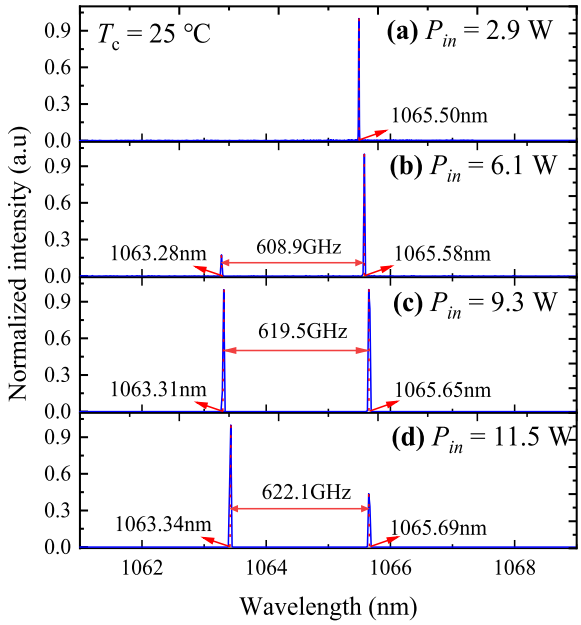

Fig. 5. The DWL spectra with the pump power of 2.9 W, 6.1 W, 9.3 W and 11.5 W at T_c = 25 °C.

dual-polarized lights are mainly due to the intracavity Brewster polarizer, which degrades the beam quality. The output beam transverse intensity profiles are depicted in the inset of Fig. 4, which exhibits the π- and σ-polarized laser signals operating in a good fundamental mode.

The evolution of the lasing spectra with pump power increasing for T_c = 25 °C is shown in Fig. 5. The laser signal only oscillates at 1065.50 nm (σ-polarized) with the pump power at 2.9 W. With the pump power increases to 6.1W, the laser signal at 1063.28 nm (π-polarized) also appeared. When the pump power reaches 9.3 W, the output intensities of the π- and σ-polarized light are maintained to be 1:1 and the wavelengths locate at 1063.31 nm and 1065.65 nm with the line widths of 0.04 nm and 0.06 nm, respectively. The wavelength separation is of 2.34 nm and the frequency separation is calculated as 0.62 THz. At the maximum pump power of 11.5 W, the output intensity of 1065.69 nm (σ-polarized) is lower than that of 1063.34 nm (π-polarized), which was resulted from the mode competition. When the pump power increases from 2.9 to 11.5 W, the wavelength of the π-polarized light shifts from 1063.28 to 1063.34 nm and the wavelength of the σ-polarized light shifts from 1065.50 to 1065.69 nm. The frequency separation of the DWL is tuned from 608.9 to 622.1 GHz. With the phonon theory by Sardar and Yow [27], the laser wavelength shifts with the pump powers varying is explained as follows. Though the temperature controlling systems are employed, the increasing of the pump power results in the increasing of the laser crystal temperature [24]. With the temperature increasing, the π- and σ-polarized ECS spectral wavelengths red shift, which causes the wavelengths of the two polarized light to red shift [28]. The different red shift rates of the two wavelengths with the laser crystal temperature change lead to the variation in the frequency separation with the temperature.

V. Conclusion

In conclusion, based on the temperature dependent ECS spectrum of the Nd:GdVO$_4$ crystal, by choosing different reflectivities of the output coupler, a power balanced Nd:GdVO$_4$ DWL with 0.6 THz frequency separation at T_c in the range of 20 °C to 40 °C is successfully realized. When the pump power of 9.3 W and T_c of 25 °C, the maximum balanced output power is 0.78 W $\times$ 2, and the frequency separation is 0.62 THz. The π- and σ-polarized laser signals operate in a good fundamental mode. Such simultaneous Nd:GdVO$_4$ DWL is desirable for scientific and practical applications, especially for the development of terahertz sources.

References

[1] A. Rolland, M. Brunel, G. Loas, L. Frein, M. Vallet, and M. Alouini, "Beat note stabilization of a 10–60 GHz dual-polarization microlaser through optical down conversion," *Opt. Exp.*, vol. 19, no. 5, pp. 4399–4404, 2011, doi: 10.1364/OE.19.004399.

[2] Y. Qiao, S. Zheng, H. Chi, X. Jin, and X. Zhang, "Electro-optically tunable microwave source based on composite-cavity microchip laser," *Opt. Exp.*, vol. 20, no. 27, pp. 29090–29095, Dec. 2012, doi: 10.1364/OE.20.029090.

[3] G. Pillet, L. Morvan, L. Ménager, A. Garcia, S. Babiel, and A. Stöhr, "Dual-frequency laser phase locked at 100 GHz," *J. Lightw. Technol.*, vol. 32, no. 20, pp. 3824–3830, Oct. 2014, doi: 10.1109/JLT.2014.2333036.

[4] E. F. Bernstein, K. T. Schomacker, L. D. Basilavecchio, J. M. Plugis, and J. D. Bhawalkar, "Treatment of acne scarring with a novel fractionated, dual-wavelength, picosecond-domain laser incorporating a novel holographic beam-splitter," *Laser Surg. Med.*, vol. 49, no. 9, pp. 796–802, 2017, doi: 10.1002/lsm.22734.

[5] K. Negishi, H. Akita, and Y. Matsunaga, "Prospective study of removing solar lentigines in asians using a novel dual-wavelength and dual-pulse width picosecond laser," *Lasers Surg. Med.*, vol. 50, no. 8, pp. 851–858, Oct. 2018, doi: 10.1002/lsm.22820.

[6] T. Wang, D. Chen, J. Yang, G. Ma, W. Yu, and X. Lin, "Safety and efficacy of dual-wavelength laser (1064 + 595 nm) for treatment of non-treated port-wine stains," *J. Eur. Acad. Dermatol Venereol*, vol. 32, no. 2, pp. 260–264, Feb. 2018, doi: 10.1111/jdv.14490.

[7] D. G. Abdelsalam, R. Magnusson, and D. Kim, "Single-shot, dual-wavelength digital holography based on polarizing separation," *Appl. Opt.*, vol. 50, no. 19, pp. 3360–3368, 2011, doi: 10.1364/AO.50.003360.

[8] T. Tahara, R. Mori, S. Kikunaga, Y. Arai, and Y. Takak, "Dual-wavelength phase-shifting digital holography selectively extracting wavelength information from wavelength-multiplexed holograms," *Opt. Lett.*, vol. 40, no. 12, pp. 2810–2813, 2015, doi: 10.1364/OL.40.002810.

[9] U. Sharma, C. -S. Kim, J. U. Kang, and N. M. Fried, "Highly stable tunable dual-wavelength Q-switched fiber laser for DIAL applications," *IEEE Photon. Technol. Lett.*, vol. 16, no. 5, pp. 1277–1279, Feb. 2004, doi: 10.1109/LPT.2004.825991.

[10] C. -K. Wang, Y. -H. Tseng, and H. -J. Chu, "Airborne dual-wavelength LiDAR data for classifying land cover," *Remote Sens.*, vol. 6, no. 1, pp. 700–715, Jan. 2014. 1. doi: 10.3390/rs6010700.

[11] N. Cao, S. Yang, S. Cao, S. Yang, and J. Shen, "Accuracy calculation for LiDAR ratio and aerosol size distribution by dual-wavelength LiDAR," *Appl. Phys.*, vol. 125, 2019, Art. no. 590, doi: 10.1007/s00339-019-2819-y.

[12] M. Tani, O. Morikawa, S. Matsuura, and M. Hangyo, "Generation of terahertz radiation by photomixing with dual- and multiple-mode lasers," *Semicond. Sci. Technol.*, vol. 20, no. 7, pp. S151–S163, 2005, doi: 10.1088/0268-1242/20/7/005.

[13] P. Zhao, S. Ragam, Y. J. Ding, and I. B. Zotova, "Compact and portable terahertz source by mixing two frequencies generated simultaneously by single solid-state laser," *Opt. Lett.*, vol. 35, no. 23, pp. 3979–3981, 2010, doi: 10.1364/OL.35.003979.

[14] P. Zhao, S. Ragam, Y. J. Ding, and I. B. Zotova, "Power scalability and frequency agility of compact terahertz source based on frequency mixing from solid-state lasers," *Appl. Phys. Lett.*, vol. 98, no. 13, Mar. 2011, Art. no. 131106, doi: 10.1063/1.3572337.

[15] A. Brenier, "Two-frequency pulsed $YLiF_4$:Nd lasing out of the principal axes and THz generation," *Opt. Lett.*, vol. 40, no. 19, pp. 4496–4499, 2015, doi: 10.1364/OL.40.004496.

[16] M. Koch, "Terahertz technology: A land to be discovered," *Opt. Photon. News*, vol. 18, no. 3, pp. 20–25, 2007, doi: 10.1364/OPN.18.3.000020.

[17] A. McKay and J. M. Dawes, "Tunable terahertz signals using a helicoidally polarized ceramic microchip laser," *IEEE Photon. Technol. Lett.*, vol. 21, no. 7, pp. 480–482, Apr. 2009, doi: 10.1109/LPT.2009.2013727.

[18] Y. P. Huang, C. Y. Cho, Y. J. Huang, and Y. F. Chen, "Orthogonally polarized dual-wavelength Nd:$LuVO_4$ laser at 1086 nm and 1089 nm," *Opt. Exp.*, vol. 20, no. 5, pp. 5644–5651, 2012, doi: 10.1364/OE.20.005644.

[19] B. Wu, P. Jiang, D. Yang, T. Chen, J. Kong, and Y. Shen, "Compact dual-wavelength Nd:$GdVO_4$ laser working at 1063 and 1065 nm," *Opt. Exp.*, vol. 17, no. 8, pp. 6004–6009, 2009, doi: 10.1364/OE.17.006004.

[20] F. Pallas, E. Herault, J. Zhou, J. F. Roux, and G. Vitrant, "Stable dual-wavelength microlaser controlled by the output mirror tilt angle," *Appl. Phys. Lett.*, vol. 99, no. 24, 2011, Art. no. 241113, doi: 10.1063/1.3669530.

[21] H. C. Liang and C. S. Wu, "Diode-pumped orthogonally polarized self-mode-locked Nd:YLF lasers subject to gain competition and thermal lensing effect," *Opt. Exp.*, vol. 25, no. 12, pp. 13697–13704, Jun. 2017, doi: 10.1364/OE.25.013697.

[22] M. Hu et al., "Microchip dual-frequency laser with well-balanced intensity utilizing temperature control," *Opt. Exp.*, vol. 24, no. 20, pp. 23383–23389, Oct. 2016, doi: 10.1364/OE.24.023383.

[23] B. Aull and H. Jenssen, "Vibronic interactions in Nd:YAG resulting in nonreciprocity of absorption and stimulated emission cross sections," *IEEE J. Quantum Electron.*, vol. 18, no. 5, pp. 925–930, May 1982, doi: 10.1109/JQE.1982.1071611.

[24] D. Xavier, P. Georges, X. Délen, and F. Balembois, "Temperature dependence of the emission cross section of Nd:YVO_4 around 1064 nm and consequences on laser operation laser operation," *J. Opt. Soc. Amer. B*, vol. 28, no. 5, pp. 972–976, 2011, doi: 10.1364/JOSAB.28.000972.

[25] T. Y. Fan and R. L. Byer, "Diode-laser-pumped solid-state lasers," *IEEE J. Quantum Electron.*, vol. 24, no. 6, pp. 895–912, Jun. 1988, doi: 10.1109/3.210.

[26] P. Laporta and M. Brussard, "Design criteria for mode size optimization in diode-pumped solid-state lasers," *IEEE J. Quantum Electron*, vol. 27, no. 10, pp. 2319–2326, Oct. 1991, doi: 10.1109/3.97276.

[27] D. K. Sardar and R. M. Yow, "Stark components of $^4F_{3/2}$, $^4I_{9/2}$ and $^4I_{11/2}$ manifold energy levels and effects of temperature on the laser transition of Nd_{3+} in YVO_4," *Opt. Mater.*, vol. 14, no. 1, pp. 5–11, 2000, doi: 10.1016/S0925-3467(99)00109-3.

[28] Y. Zhang et al., "Experimental investigation on the Y-type cavity tunable dual-wavelength laser based on neodymium-doped vanadate crystals," *Opt. Commun.*, vol. 495, Sep. 2021, Art. no. 127089, doi: 10.1016/j.optcom.2021.127089.